

# Model and probe measurements of inductively coupled CF<sub>4</sub> discharges

T. Kimura<sup>a)</sup> and K. Ohe

*Department of Systems Engineering, Nagoya Institute of Technology, Nagoya 466-8555, Japan*

(Received 11 March 2002; accepted for publication 10 May 2002)

A global model for electronegative plasma, in which the negative ion distribution is assumed to be a parabolic profile in the axial direction with a flat central region and a similar edge profile in the radial direction in the electronegative region, is applied to study the power and pressure dependences of plasma parameters in low-pressure CF<sub>4</sub> discharges. The electron density increases approximately linearly with the power. The electron temperature also increases with the power due to the decrease in neutral number density with increase in power, resulting in the increase in plasma potential. The density of CF<sub>3</sub><sup>+</sup> is a weak function of the power, while the densities of CF<sub>2</sub><sup>+</sup>, CF<sup>+</sup>, and F<sup>+</sup>, which are strongly correlated to the densities of the respective radicals, depend on the power. On the other hand, the decrease in electron temperature with the pressure significantly results in a decrease in the degree of dissociation. The electron density also decreases gradually with the pressure except for the case of pressure lower than 5 mTorr. The densities of CF<sub>2</sub><sup>+</sup>, CF<sup>+</sup>, and F<sup>+</sup> decrease gradually with the pressure at pressures higher than 5 mTorr, while the density of CF<sub>3</sub><sup>+</sup> increases gradually with the pressure. The electron energy probability function (EEPF) is measured with a Langmuir probe in an inductively coupled rf (13.56 MHz) CF<sub>4</sub> discharge over a pressure range from 2 to 30 mTorr, while keeping the power injected into the plasma at about 70 W. The measured EEPFs are approximately Maxwellian at any pressure, although there is a slight deviation from a Maxwellian distribution at pressures higher than 10 mTorr. The results estimated from the measured EEPF are compared to the model and show reasonably good agreement. © 2002 American Institute of Physics. [DOI: 10.1063/1.1491023]

## I. INTRODUCTION

Carbon tetrafluoride (CF<sub>4</sub>) with a mixture of oxygen and hydrogen is commonly used in silicon and silicon dioxide etching processes for manufacturing microelectronic devices. For plasma processing applications, CF<sub>4</sub> serves as a source of reactive species which are responsible for surface reaction in various etching and deposition processes.

Earlier on, high-pressure and low-density CF<sub>4</sub> plasmas were produced in capacitively coupled radio frequency (rf) discharges in the pressure range of hundreds of mTorr. Many experimental and theoretical studies<sup>1–12</sup> of capacitively coupled rf CF<sub>4</sub> discharges have been reported, so important physical and chemical processes in plasma have been understood. In experimental studies, neutral species such as CF<sub>2</sub> and CF radicals were measured using a laser-induced fluorescence method,<sup>3</sup> and the electron and negative ion densities in afterglow CF<sub>4</sub> plasmas were measured by a microwave cavity method and a laser photodetachment technique.<sup>4,5</sup> On the other hand, modeling of the capacitively coupled rf CF<sub>4</sub> discharge<sup>1,2,6,7</sup> has concentrated on chemical kinetics and surface reactions rather than discharge physics. However, modeling of discharge physics<sup>8–12</sup> has progressed, and important physical and chemical processes in plasma have been understood.

Recently, low-pressure and high-density CF<sub>4</sub> plasma have been produced in inductively coupled discharges and electron cyclotron resonance discharges. Differences in the

operating conditions between capacitively and inductively coupled discharges may cause different behaviors in the plasma chemistry. In CF<sub>4</sub> inductive discharges, the surface loss coefficients of neutral radicals on the surfaces of the plasma reactor,<sup>13</sup> which strongly affect the plasma composition, and the electron energy distribution function (EEDF)<sup>14,15</sup> that is essential to know the gas-phase reaction rates have been investigated. The neutral number densities were measured using appearance potential mass spectrometry,<sup>15,16</sup> and the ion fluxes and energy distributions were also measured using mass spectrometry.<sup>17,18</sup> The EEDF measured in CF<sub>4</sub> inductively coupled discharge was approximately a Maxwellian distribution at pressures lower than 30 mTorr, resulting in the simplification of models such as global and fluid models due to the validity of the Maxwellian EEDF assumption. The results of fluid models, which couple the plasma generation and transport to the gas flow and heating, agree with the probe measurements in the case of electron temperature, although there is a significant difference in electron density.<sup>19,20</sup> Here, we investigate plasma parameters of low-pressure and high-density CF<sub>4</sub> plasmas using a global model.

In a previous global model for electronegative gas, all quantities are assumed to be uniform over the discharge to simplify the complexity. Then, the loss flux of positive ions to the wall is assumed to be calculated using flux factors<sup>21</sup> that have been determined separately for one-dimensional plane-parallel and cylindrical electropositive plasmas. This assumption is applicable to weakly electronegative discharges, such as O<sub>2</sub>/Ar mixtures<sup>22,23</sup> and CF<sub>4</sub>/Ar mixtures.<sup>24</sup>

<sup>a)</sup>Electronic mail: kimura@system.nitech.ac.jp

TABLE I. Reactions considered in the model.

Reaction	Rate coefficients ( $\text{m}^3 \text{s}^{-1}$ )	Reference
$\text{CF}_4 + e \rightarrow \text{CF}_3 + \text{F} + e$	$k_1 = 1.38 \times 10^{-14} \exp(-16.0/T_e)$	27
$\text{CF}_4 + e \rightarrow \text{CF}_2 + 2\text{F} + e$	$k_2 = 2.22 \times 10^{-16} T_e^{0.99} \exp(-14.77/T_e)$	19
$\text{CF}_4 + e \rightarrow \text{CF} + 3\text{F} + e$	$k_3 = 7.29 \times 10^{-15} / T_e^{0.165} \exp(-28.26/T_e)$	19
$\text{CF}_3 + e \rightarrow \text{CF}_2 + \text{F} + e$	$k_4 = 1.25 \times 10^{-15} T_e^{0.5}$	12
$\text{CF}_2 + e \rightarrow \text{CF} + \text{F} + e$	$k_5 = 1.25 \times 10^{-15} T_e^{0.5}$	12
$\text{CF}_3 + \text{F} \rightarrow \text{CF}_4$	$k_6 = 2.3 \times 10^{-19} \times p(\text{mTorr})$	2
$\text{CF}_2 + \text{F} \rightarrow \text{CF}_3$	$k_7 = 9 \times 10^{-22} \times p(\text{mTorr})$	2
$\text{CF}_4 + e \rightarrow \text{CF}_3^+ + \text{F} + 2e$	$k_8 = 9.36 \times 10^{-14} \exp(-20.4/T_e)$	28
$\text{CF}_4 + e \rightarrow \text{CF}_2^+ + 2\text{F} + 2e$	$k_9 = 1.27 \times 10^{-14} \exp(-29.0/T_e)$	28
$\text{CF}_4 + e \rightarrow \text{CF}^+ + 3\text{F} + 2e$	$k_{10} = 1.04 \times 10^{-14} \exp(-33.3/T_e)$	28
$\text{CF} + \text{F} \rightarrow \text{CF}_2$	$k_{11} = 9.6 \times 10^{-24} \times p(\text{mTorr})$	2
$\text{CF}_3 + e \rightarrow \text{CF}_3^+ + 2e$	$k_{12} = 8 \times 10^{-15} \exp(-12.2/T_e)$	29
$\text{CF}_2 + e \rightarrow \text{CF}_2^+ + 2e$	$k_{13} = 2.5 \times 10^{-14} \exp(-12.2/T_e)$	29
$\text{CF} + e \rightarrow \text{CF}^+ + 2e$	$k_{14} = 2.5 \times 10^{-14} \exp(-15.3/T_e)$	29
$\text{CF}_4 + e \rightarrow \text{F}^- + \text{CF}_3$	$k_{15} = 5.9 \times 10^{-16} T_e^{-1} \exp(-5.2/T_e)$	28
$\text{CF}_3^+ + e \rightarrow \text{CF}_3$	$k_{16} = 9.6 \times 10^{-13}$	9
$\text{CF}_3 + \text{F}^- \rightarrow \text{CF}_4 + e$	$k_{17} = 5 \times 10^{-16}$	9
$\text{X}^+ + \text{F}^- \rightarrow \text{X} + \text{F}$	$k_{18} = 1 \times 10^{-13}$	30
$\text{CF}_3 + e \rightarrow \text{CF}_2^+ + \text{F} + 2e$	$k_{19} = 2.20 \times 10^{-14} \exp(-18.6/T_e)$	31
$\text{CF}_2 + e \rightarrow \text{CF}^+ + \text{F} + 2e$	$k_{20} = 2.33 \times 10^{-14} \exp(-17.0/T_e)$	31
$\text{CF}_3 + e \rightarrow \text{CF}_2 + \text{F}^-$	$k_{21} = 5.9 \times 10^{-16} T_e^{-1} \exp(-5.2/T_e)$	(assumed)
$\text{CF}_2 + e \rightarrow \text{CF} + \text{F}^-$	$k_{22} = 5.9 \times 10^{-16} T_e^{-1} \exp(-5.2/T_e)$	(assumed)
$\text{F} + e \rightarrow \text{F}^+ + 2e$	$k_{23} = 1.3 \times 10^{-14} \exp(-16.5/T_e)$	32,33
$\text{F} + \text{F} \rightarrow \text{F}_2$	$k_{24} = 6.77 \times 10^{-40} (\text{m}^6 \text{s}^{-1})$	30
$\text{F}_2 + e \rightarrow \text{F}^- + \text{F}$	$k_{25} = 4.5 \times 10^{-15} T_e^{-1.35} \exp(-0.15/T_e)$	33
$\text{F}_2 + e \rightarrow \text{F} + \text{F} + e$	$k_{26} = 1.18 \times 10^{-14} \exp(-5.77/T_e)$	33
$\text{CF}_3^+ \rightarrow \text{CF}_3$	$2 U_{B, \text{CF}_3} (R^2 h_L + RL h_R) / R^2 L (\text{s}^{-1})$	
$\text{CF}_2^+ \rightarrow \text{CF}_2$	$2 U_{B, \text{CF}_2} (R^2 h_L + RL h_R) / R^2 L (\text{s}^{-1})$	
$\text{CF}^+ \rightarrow \text{CF}$	$2 U_{B, \text{CF}} (R^2 h_L + RL h_R) / R^2 L (\text{s}^{-1})$	
$\text{F}^+ \rightarrow \text{F}$	$2 U_{B, \text{F}} (R^2 h_L + RL h_R) / R^2 L (\text{s}^{-1})$	
$\text{CF}_3 + (\text{wall}) \rightarrow \text{loss}$	$[\Lambda^2 / D_{\text{CF}_3} + 2\pi R^2 L (2 - \gamma) / Sv_{\text{th}} \gamma]^{-1} (\text{s}^{-1}) (\gamma = 0.017)$	12,13
$\text{CF}_2 + (\text{wall}) \rightarrow \text{loss}$	$[\Lambda^2 / D_{\text{CF}_2} + 2\pi R^2 L (2 - \gamma) / Sv_{\text{th}} \gamma]^{-1} (\text{s}^{-1}) (\gamma = 0.02)$	12,13
$\text{CF} + (\text{wall}) \rightarrow \text{loss}$	$[\Lambda^2 / D_{\text{CF}} + 2\pi R^2 L (2 - \gamma) / Sv_{\text{th}} \gamma]^{-1} (\text{s}^{-1}) (\gamma = 0.036)$	12,13
$\text{F} + (\text{wall}) \rightarrow \text{loss}$	$[\Lambda^2 / D_{\text{F}} + 2\pi R^2 L (2 - \gamma) / Sv_{\text{th}} \gamma]^{-1} (\text{s}^{-1}) (\gamma = 0.02)$	12,13
$S = 2\pi(R^2 + RL)$		
$v_{\text{th}}$ : thermal velocity		

However, in one-dimensional (1D) analysis,<sup>25</sup> it was found that the plasma in weakly electronegative discharges is divided into an electronegative core, electropositive edge, and a sheath, and the approximation of a parabolic negative ion profile in the core is applicable over a considerable range of electronegativity  $\alpha_0$  [ $\alpha_0 \equiv n_-(0)/n_e$ ], with  $n_-(0)$  the central negative ion density and  $n_e$  the electron density. The loss flux of positive ions to the wall was also calculated using a flux factor for plane-parallel electronegative discharges and was significantly different from that for electropositive plasmas.

Recently we proposed an improved global model<sup>26</sup> for a finite cylindrical electronegative plasma, where the negative ion distribution is assumed to be a parabolic profile in the axial direction with a flat central region and a similar edge profile in the radial direction in the electronegative core, and applied the model to inductively coupled oxygen discharges. In the model, the loss flux of positive ions to the wall is larger and therefore the calculated electron density is lower than that obtained from the previous (uniform) global model, resulting in significantly better agreement between the experimental and theoretical electron densities.

In the present article we apply the improved model for finite cylindrical electronegative discharge to investigate power and pressure dependences of the plasma parameters in low-pressure  $\text{CF}_4$  discharges and compare the results with experimental values measured by a Langmuir probe over a range of pressure.

## II. DESCRIPTION OF GLOBAL MODEL

A global model for electronegative plasma, in which the negative ion distribution is assumed to be a parabolic profile in the axial direction with a flat central region and a similar edge profile in the radial direction in the electronegative core, is applied to  $\text{CF}_4$  plasma in a cylindrical chamber of radius  $R$  and length  $L$ . The reactions and rate coefficients considered in the model are listed in Table I. Six neutral species ( $\text{CF}_4$ ,  $\text{CF}_3$ ,  $\text{CF}_2$ ,  $\text{CF}$ ,  $\text{F}$ , and  $\text{F}_2$ ) and six charged species (electrons,  $\text{CF}_3^+$ ,  $\text{CF}_2^+$ ,  $\text{CF}^+$ ,  $\text{F}^+$ , and  $\text{F}^-$ ) in the  $\text{CF}_4$  discharge are considered, and all neutral species are assumed to be uniform over the chamber. Electrons which have a Maxwellian energy distribution with electron temperature  $T_e$  are also assumed to be uniform over the chamber, since the

plasma dimensions with radius  $r_p$  and length  $2\ell_p$  are approximately equal to the chamber dimensions due to the thin sheath for inductive discharges. On the other hand, negative ions are assumed to be trapped in the cylindrical electronegative core of radius  $r_-$  and length  $2\ell_-$ , where  $r_- = R - \ell_p + \ell_-$ . According to a previous paper,<sup>26</sup> the negative ion distribution  $n_-$  can be approximated as

$$n_-(r, z) = \begin{cases} n_e \alpha_0 \left( 1 - \frac{z^2}{\ell_-^2} \right) & \left| r \leq (r_p - \ell_p) \right. \\ n_e \alpha_0 \left( 1 - \frac{(r - r_- + \ell_-)^2}{\ell_-^2} \right) & \left. r_p - \ell_p < r < r_- \right. \end{cases} \quad (1)$$

$$\times \left( 1 - \frac{z^2}{\ell_-^2} \right) \Big|_{r_p - \ell_p < r < r_-},$$

where  $n_e$  is the electron density and the electronegativity  $\alpha_0$  is given as  $\alpha_0 = n_-(0)/n_e$ . Although defining the electronegative region by a single scale in plasmas that include more negative ions is not straightforward, the approximation of  $n_-$  is useful in  $\text{CF}_4$  plasmas because the density of  $\text{F}^-$  is much larger than that of  $\text{CF}_3^-$ . All positive ion species, which are assumed to have the same profile, must satisfy the quasineutrality,

$$n_e + n_- = n_{\text{CF}_3^+} + n_{\text{CF}_2^+} + n_{\text{CF}^+} + n_{\text{F}^+},$$

where  $n_{\text{CF}_3^+}$ ,  $n_{\text{CF}_2^+}$ ,  $n_{\text{CF}^+}$ , and  $n_{\text{F}^+}$  are the respective positive ion densities.

For electronegativity  $\alpha_0 \leq 10$ , the plasma is stratified into an electronegative core and an electropositive edge. The density  $n_e$  is not constant in the electropositive edge, although the electron density profile within the electronegative core is quite uniform. Actually, electron density  $n_e$  falls relatively abruptly near the sheaths to edge values  $n_{e\ell} = h_\ell n_e$  and  $n_{er} = h_r n_e$  at the axial and circumferential sheaths, where the velocity for positive ion  $X$  can reach the Bohm velocity  $U_{B,X} = (eT_e/M_X)^{1/2}$ . The  $h_\ell$  and  $h_r$  factors are expressed as<sup>26</sup>

$$h_\ell = \left( \frac{a_\ell + [I_{+z}(\ell_-)/(\pi r_p^2 n_e u_B)]^3}{1 + a_\ell} \right)^{1/3} \quad (2)$$

and

$$h_r = \left( \frac{a_r + [I_{+r}(r_-)/(2\pi r_p \ell_p n_e u_B)]^3}{1 + a_r} \right)^{1/3}, \quad (3)$$

where

$$a_\ell = \frac{2\nu_{iz}\lambda}{\pi u_B} \left( \frac{r_p h_\ell}{r_p h_\ell + 2\ell_p h_r (1 - \ell_-/\ell_p)} \right),$$

$$a_r = \frac{\nu_{iz}\lambda}{\pi u_B} \left( \frac{2\ell_p h_r}{r_p h_\ell (1 - \ell_-/\ell_p) + 2\ell_p h_r} \right).$$

The ionization frequency  $\nu_{iz}$  is approximately given as the sum of the respective ionization frequency which means the product of the ionization rate listed in Table I with the respective density of the neutral species. The  $z$ -directed and  $r$ -directed total particle currents  $I_{+z}(\ell_-)$  and  $I_{+r}(r_-)$ ,

which emerge from the EN core, are expressed with the notation of the ambipolar diffusion coefficients  $\bar{D}_{a+}$  averaged in the EN core as,

$$I_{+z}(\ell_-) = \frac{2\bar{D}_{a+} n_e \alpha_0 \pi}{\ell_-} \left( r_-^2 - \frac{2}{3} r_- \ell_- + \frac{1}{6} \ell_-^2 \right), \quad (4)$$

$$I_{+r}(r_-) = 2\bar{D}_{a+} n_e \alpha_0 \pi \frac{4}{3} r_-. \quad (5)$$

The mean free path  $\lambda$  is given by

$$\frac{1}{\lambda} = \sum_{x=1}^4 [\text{CF}_x] \sigma_{\text{CF}_x} + [\text{F}] \sigma_{\text{F}} + [\text{F}_2] \sigma_{\text{F}_2},$$

where  $\sigma_{\text{CF}_x}$ ,  $\sigma_{\text{F}}$ , and  $\sigma_{\text{F}_2}$  refer to the total ion-neutral collision cross sections. Since the detail cross section data for each ion-neutral is not present, we assume the mean free path for all positive ions are the same for simplicity. The cross section  $\sigma_{\text{CF}_x}$  is estimated as  $1.5 \times 10^{-18} \text{ m}^2$  from the mobility used in Ref. 9, and  $\sigma_{\text{F}}$  and  $\sigma_{\text{F}_2}$  are assumed to be  $5 \times 10^{-19} \text{ m}^2$ . Because we assume the profiles are the same for all positive ion species, we divide the total flux into a flux of each species in proportion to the ratio of the species density to the total density.

The diffusional loss of radicals to the wall is estimated by the effective loss rate. The effective loss rate  $X_{\text{loss}}$  for radical  $X$  is given by

$$X_{\text{loss}} = [\Lambda^2/D_X + 2(\pi R^2 L)(2 - \gamma)/S v_{\text{th}} \gamma]^{-1}, \quad (6)$$

where  $D_X$  is the neutral diffusion coefficient,  $\gamma$  the sticking coefficient on the wall,  $S$  the surface area of the chamber, and the effective diffusion length  $\Lambda$  is given by

$$\Lambda^{-2} = \left( \frac{\pi}{L} \right)^2 + \left( \frac{2.405}{R} \right)^2.$$

The values of  $D_X$  and  $\gamma$  for each radical are referred in Refs. 12 and 13, respectively.

Considering the reactions shown in Table I and the profiles described above, we can write a set of equations for the global model, in which the particle balance equation for the total of positive ions over one-half of the symmetric EN core is included in addition to the particle conservation equations and the energy conservation equation. Since the equation set is expressed in terms of average quantities, rather than peak quantities, we introduce the average electronegativity over the EN region and average densities over the entire plasma volume as,

$$\bar{\alpha} = \frac{1}{\pi r_-^2 \ell_- n_e} \int_0^{r_-} 2\pi r dr \int_0^{\ell_-} dz n_-(r, z)$$

$$= \alpha_0 \frac{2}{3} \left( 1 - \frac{2}{3} \frac{\ell_-}{r_-} + \frac{1}{6} \frac{\ell_-^2}{r_-^2} \right), \quad (7)$$

$$[\text{F}^-] = n_e \bar{\alpha} \frac{2r_-^2 \ell_-}{R^2 L}, \quad (8)$$

$$[\text{CF}_3^+] + [\text{CF}_2^+] + [\text{CF}^+] + [\text{F}^+] = n_e \left( \bar{\alpha} \frac{2r_-^2 \ell_-}{R^2 L} + 1 \right). \quad (9)$$

As examples of positive and negative ion species, we show the particle equations for  $\text{CF}_3^+$  and  $\text{F}^-$ :

$$\begin{aligned} \frac{d[\text{CF}_3^+]}{dt} = & [\text{CF}_4]n_e k_8 + [\text{CF}_3]n_e k_{12} - [\text{CF}_3^+]n_e k_{16} \\ & - I_{\text{rec}} \left( \frac{2}{\pi R^2 L} \right) \frac{[\text{CF}_3^+]}{([\text{CF}_3^+] + [\text{CF}_2^+] + [\text{CF}^+] + [\text{F}^+])} \\ & - \left( \frac{[\text{CF}_3^+]}{n_e + [\text{F}^-]} \right) n_e \text{CF}_{3\text{loss}}, \end{aligned} \quad (10)$$

$$\begin{aligned} \frac{d[\text{F}^-]}{dt} = & [\text{CF}_4]n_e k_{15} + [\text{CF}_3]n_e k_{21} + [\text{CF}_2]n_e k_{22} \\ & + [\text{F}_2]n_e k_{25} \\ & - I_{\text{rec}} \left( \frac{2}{\pi R^2 L} \right) - [\text{CF}_3][\text{F}^-]k_{17}, \end{aligned} \quad (11)$$

where

$$\begin{aligned} I_{\text{rec}} = & 2\pi \int_0^{\ell_-} dz \int_0^{r_-} r dr k_{18} n_+(r, z) n_-(r, z) \\ = & k_{18} n_e^2 \pi \ell_- \left[ \frac{8}{15} \alpha_0^2 \left( r_-^2 - \frac{14}{15} r_- \ell_- + \frac{4}{15} \ell_-^2 \right) \right. \\ & \left. + \frac{2}{3} \alpha_0 \left( r_-^2 - \frac{2}{3} r_- \ell_- + \frac{1}{6} \ell_-^2 \right) \right] \end{aligned} \quad (12)$$

is the volume recombination flux over one-half of the EN core. As examples of neutral species, we show the equations for  $\text{CF}_4$  and  $\text{CF}_3$ :

$$\begin{aligned} \frac{d[\text{CF}_4]}{dt} = & \left( \frac{Q_f}{\pi R^2 L} \right) - [\text{CF}_4]n_e k_1 - [\text{CF}_4]n_e k_2 - [\text{CF}_4]n_e k_3 + [\text{CF}_3][\text{F}]k_6 - [\text{CF}_4]n_e (k_8 + k_9 + k_{10}) - [\text{CF}_4]n_e k_{15} + [\text{CF}_3] \\ & \times [\text{F}^-]k_{17} - [\text{CF}_4] \frac{S_p}{\pi R^2 L}, \end{aligned} \quad (13)$$

$$\begin{aligned} \frac{d[\text{CF}_3]}{dt} = & [\text{CF}_4]n_e k_1 - [\text{CF}_3]n_e k_4 - [\text{CF}_3][\text{F}]k_6 + [\text{CF}_2][\text{F}]k_7 - [\text{CF}_3]n_e k_{12} + [\text{CF}_4]n_e k_{15} + [\text{CF}_3^+]n_e k_{16} - [\text{CF}_3][\text{F}^-]k_{17} \\ & - [\text{CF}_3]n_e k_{19} - [\text{CF}_3]n_e k_{21} - [\text{CF}_3]\text{CF}_{3\text{loss}} - [\text{CF}_3] \frac{S_p}{\pi R^2 L} + \left( \frac{[\text{CF}_3^+]}{n_e + [\text{F}^-]} \right) n_e \text{CF}_{3\text{loss}} \\ & + I_{\text{rec}} \left( \frac{2}{\pi R^2 L} \right) \frac{[\text{CF}_3^+]}{([\text{CF}_3^+] + [\text{CF}_2^+] + [\text{CF}^+] + [\text{F}^+])}, \end{aligned} \quad (14)$$

where  $Q_f$  corresponds to the number density of  $\text{CF}_4$  flowing into the chamber per second and  $S_p$  is the pumping speed. We can write the particle equations for other ions and neutrals in a similar manner.

The energy balance equation assumes that all power injected into the plasma is dissipated through collision processes between electrons and neutral species and the kinetic energies of ions and electrons flowing into the walls.

$$\begin{aligned} \frac{3}{2} \frac{d(en_e T_e)}{dt} = & \frac{P_{\text{abs}}}{\pi R^2 L} - e \mathcal{E}_c^{(\text{CF}_4)} k_8 [\text{CF}_4]n_e - e \mathcal{E}_c^{(\text{CF}_3)} k_{12} [\text{CF}_3]n_e - e \mathcal{E}_c^{(\text{CF}_2)} k_{13} [\text{CF}_2]n_e - e \mathcal{E}_c^{(\text{CF})} k_{14} [\text{CF}]n_e - e \mathcal{E}_c^{(\text{F})} k_{23} [\text{F}]n_e \\ & - e \mathcal{E}_c^{(\text{F}_2)} k_{i_z, \text{F}_2} [\text{F}_2]n_e - n_e e (\mathcal{E}_e + \mathcal{E}_i) \frac{([\text{CF}_3^+]\text{CF}_{3\text{loss}} + [\text{CF}_2^+]\text{CF}_{2\text{loss}} + [\text{CF}^+]\text{CF}_{\text{loss}} + [\text{F}^+]\text{F}_{\text{loss}})}{([\text{CF}_3^+] + [\text{CF}_2^+] + [\text{CF}^+] + [\text{F}^+])}, \end{aligned} \quad (15)$$

where  $\mathcal{E}_c^{(\text{CF}_{x(x=1,2,3,4)})}$ ,  $\mathcal{E}_c^{(\text{F})}$ , and  $\mathcal{E}_c^{(\text{F}_2)}$  are the respective collisional energy losses per electron-ion pair created, which include all excitation energies such as vibrational, dissociative, and electronic excitations,  $\mathcal{E}_e = 2T_e$  is the electron energy lost to the walls, and  $\mathcal{E}_i = V_{\text{sh}} + T_e/2$  is the energy lost to ions accelerating through the sheath. The energy  $\mathcal{E}_c^{(\text{CF}_4)}$  is calculated by using the cross section data summarized by Christorou *et al.*<sup>27,28</sup> while  $\mathcal{E}_c^{(\text{CF}_{x(x=1,2,3)})}$  is calculated by adding the vibrational collisions (not indirect vibrational collision), which are assumed to have the same rate coefficients as  $\text{CF}_4$ ,

to the reactions listed in Table I. We show  $\mathcal{E}_c^{(\text{CF}_4)}$  as an example of collisional energy losses per electron-ion pair created. The energy  $\mathcal{E}_c^{(\text{CF}_4)}$  is given as

$$\begin{aligned} \mathcal{E}_c^{(\text{CF}_4)} = & \epsilon_{i_z(\text{CF}_4)} + \sum \epsilon_{\text{vib}} \frac{k_{\text{vib}}}{k_8} + \epsilon_{\text{indir,vib}} \frac{k_{\text{indir,vib}}}{k_8} \\ & + \sum \epsilon_{\text{diss}} \frac{k_{\text{diss}}}{k_8} + \frac{3m}{M_{\text{CF}_4}} \frac{k_{\text{elas}}}{k_8} T_e, \end{aligned} \quad (16)$$

where  $\epsilon_{\text{vib}}$ ,  $\epsilon_{\text{indir,vib}}$ , and  $\epsilon_{\text{diss}}$  are the threshold energies of the vibrational and indirect vibrational excitations, and dis-

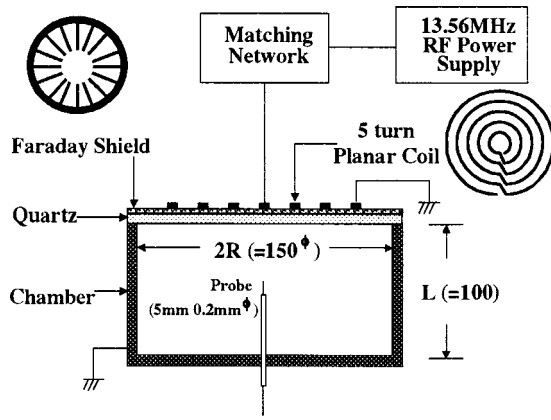


FIG. 1. Schematic diagram of experimental setup.

sociation in eV, respectively, and  $\epsilon_{iz}(\text{CF}_4)$  is given as  $\epsilon_{iz}(\text{CF}_4) = \sum_{j=8}^{10} \epsilon_{iz,j}(k_j/k_8)$  with the notation of ionization threshold energy  $\epsilon_{iz,j}$  for the reaction  $j$ . Moreover, we calculated  $\mathcal{E}_c^{(F)}$  and  $\mathcal{E}_c^{(F_2)}$  from the rate coefficients described in Ref. 33. The sheath edge voltage drop  $V_{sh}$  is given as  $V_{sh} = T_e/2 \ln(M/2\pi m)$  with the notations of the effective positive ion mass  $M$  and electron mass  $m$  because the sheath is thin compared to the separation of the inductive exciting coil from the plasma and an electrostatic shield is used.

Since the length  $\ell_-$  is introduced in the model, one additional equation is required. According to a previous paper,<sup>26</sup> we introduce a balance equation over one-half of the symmetric EN region. The balance equation for the total of positive ions over one-half of the symmetric EN region can be written as

$$v_{iz} n_e \pi r_-^2 \ell_- = I_{\text{rec}, \text{CF}_3^+} + I_{\text{rec}} + I_{+z}(\ell_-) + I_{+r}(r_-), \quad (17)$$

where  $I_{\text{rec}, \text{CF}_3^+}$  is the flux of volume recombination between electrons and  $\text{CF}_3^+$  over one-half of the EN core, and given as,

$$I_{\text{rec}, \text{CF}_3^+} = n_e k_{16} \pi r_-^2 \ell_- [\text{CF}_3^+] \frac{\bar{\alpha} + 1}{\bar{\alpha} (2r_-^2 \ell_-)/(R^2 L) + 1}, \quad (18)$$

The equations for each particle and power balance and Eq. (17) are then solved by use of the Runge–Kutta numerical method to obtain an equilibrium (the left-hand sides equal zero).

### III. EXPERIMENT

A schematic diagram of the experimental apparatus is shown in Fig. 1. The stainless steel chamber was cylindrical, 15 cm in inner diameter and 10 cm in length, with a quartz plate of 1.0 cm thickness placed at the upper end of the chamber. The discharge was sustained by an azimuthal electric field induced by the rf coil current supplied to a planar five-turn coil from a power source connected to an L-type capacitive matching network. The planar coil mounted at about 0.4 cm above the quartz plate was concentric in the center of the chamber to maintain the discharge symmetry. An electrostatic shield practically eliminated the capacitive coupling between the coil and the plasma, resulting in suppression of any rf plasma potential fluctuation. A cylindrical probe 5 mm in length and 0.2 mm in diameter was installed at the chamber center. The power  $P_{\text{abs}}$  injected into the plasma was estimated by subtracting the transmitted power without plasma from that with plasma at the same current.

The EEDF  $F(\epsilon)$  was measured by detecting the second derivative  $i_p''$  of the probe current  $i_p$  with respect to the probe bias voltage  $V_p$ , according to the Druyvesteyn formula<sup>34</sup>

$$F(\epsilon) = \frac{4}{A e^2 n_e} \left( \frac{m}{2e} \right)^{1/2} V^{1/2} i_p'', \quad (19)$$

where  $\epsilon$  is the electron energy in eV,  $A$  is the probe area, and  $V$  is the difference between the plasma potential, which is determined as  $V_p$  corresponding to  $i_p'' = 0$ , and  $V_p$ . The electron energy probability function (EEDF)  $f(\epsilon)$  can be then deduced as

$$f(\epsilon) = F(\epsilon) \epsilon^{-1/2}. \quad (20)$$

The electron density is found by integration over the distribution. The EEDF detection system is described in a previously published paper.<sup>24</sup>

### IV. RESULTS AND DISCUSSION

#### A. Results of model

The calculated power dependence of plasma parameters for the pressure of 15 mTorr, which corresponds to the pressure with the discharge off, is shown in Tables II and III, where  $Q_f = 20$  sccm,  $R = 7.5$  cm, and  $L = 10$  cm. The electron density increases approximately linearly with power. The electron temperature, which is sensitive to the neutral number density, also increases with the power due to the decrease in neutral number density with increase in power, resulting in the increase in plasma potential. The variation of

TABLE II. Power dependence of plasma parameters for charged species at  $p = 15$  mTorr, where all densities are in units of  $10^{16} \text{ m}^{-3}$ .

$P_{\text{abs}}$ (W)	$n_e$	$T_e$ (eV)	$V_{sh}$ (V)	$\alpha_0$	$\ell_-/\ell_p$	$[\text{CF}_3^+]$	$[\text{CF}_2^+]$	$[\text{CF}^+]$	$[\text{F}^+]$
30	1.51	3.19	15.8	5.51	0.743	3.03	0.252	0.0426	0.0426
50	2.56	3.34	16.5	4.00	0.719	3.82	0.621	0.137	0.142
70	3.75	3.49	17.3	3.17	0.690	4.29	1.12	0.315	0.319
100	5.86	3.72	18.4	2.37	0.631	4.44	2.04	0.808	0.821
120	7.49	3.88	19.2	1.98	0.586	4.24	2.67	1.31	1.35
150	10.0	4.10	20.3	1.54	0.529	3.73	3.47	2.26	2.37



TABLE III. Power dependence of plasma parameters for neutral species at  $p = 15$  mTorr, where all densities are in units of  $10^{18} \text{ m}^{-3}$ .

$P_{\text{abs}} \text{ (W)}$	$[\text{CF}_4]$	$[\text{CF}_3]$	$[\text{CF}_2]$	$[\text{CF}]$	$[\text{F}]$	$[\text{F}_2]$
30	373	10.3	3.07	0.62	10.6	0.573
50	305	13.1	5.58	1.95	19.9	1.08
70	241	14.3	7.57	3.96	30.2	1.48
100	156	14.2	9.19	7.91	46.7	1.74
120	112	13.2	9.34	10.7	56.6	1.69
150	69.8	11.3	8.74	14.0	67.7	1.47

$\alpha$  is somewhat faster than the variation proportional to  $n_e^{-1/2}$ , which is predicted in the model,<sup>25</sup> due to the decrease in  $\text{CF}_4$  density with the power. The density of  $\text{CF}_3^+$ , which is formed by dissociative ionization of  $\text{CF}_4$  and direct ionization of  $\text{CF}_3$ , is a weak function of the power due to the decrease in  $\text{CF}_4$  density with the increase in power. The density of  $\text{CF}_2^+$ , which is mainly formed by direct ionization of  $\text{CF}_2$  and dissociative ionization of  $\text{CF}_3$ , is approximately proportional to  $n_e$  at a power higher than 70 W because the densities of  $\text{CF}_3$  and  $\text{CF}_2$  are not strongly power-dependent due to the increase in the dissociation for  $\text{CF}_3$  and  $\text{CF}_2$  with the power. The variation of density of  $\text{CF}^+$ , which is mainly formed by the dissociative ionization of  $\text{CF}_2$  and direct ionization of  $\text{CF}$ , is similar to that of  $\text{F}^+$ . The variation of  $\text{CF}^+$  and  $\text{F}^+$  densities with the power is faster than that of  $\text{CF}_2^+$  because  $\text{CF}$  and  $\text{F}$  densities are increased functions of the power. The power dependence of the respective number densities indicates agreement with the experiment,<sup>15</sup> although a significant difference still remains between the measured and calculated densities. In particular, the predicted ratio of  $\text{F}$  density to the total neutral number density is much larger than the experiment<sup>15</sup> at high power, resulting in a large difference between measured and calculated  $\text{F}^+$  densities. Further research into reaction mechanisms of the  $\text{F}$  atom will be required.

In Tables IV and V we present numerical results over a range of pressures from  $p = 2$  to 30 mTorr for a power of 70 W, where  $Q_f = 20$  sccm,  $R = 7.5$  cm, and  $L = 10$  cm. The decrease in electron temperature with the pressure is significantly responsible for the decrease in the degree of dissociation. The electron density also decreases gradually with the pressure except in the case of pressure lower than 5 mTorr. The pressure dependence of electron temperature and its density may result in weak pressure dependence of  $\text{CF}_3$  and  $\text{CF}_2$  densities, and pressure dependence of  $\text{CF}$  and  $\text{F}$  densities

TABLE V. Pressure dependence of plasma parameters for neutral species with  $P_{\text{abs}} = 70$  W, where all densities are in units of  $10^{18} \text{ m}^{-3}$ .

$p \text{ (mTorr)}$	$[\text{CF}_4]$	$[\text{CF}_3]$	$[\text{CF}_2]$	$[\text{CF}]$	$[\text{F}]$	$[\text{F}_2]$
2	26.0	9.42	4.68	2.81	23.3	0.09
3	37.2	10.8	5.75	3.69	28.4	0.19
5	60.4	12.3	6.92	4.59	33.4	0.42
8	102	13.5	7.66	4.90	35.2	0.76
12	174	14.2	7.79	4.49	33.1	1.19
18	316	14.3	7.22	3.44	27.3	1.73
25	509	13.8	6.32	2.50	21.5	2.18
30	655	13.4	5.76	2.05	18.5	2.41

which is similar to that of  $n_e$ . Therefore the densities of  $\text{CF}_2^+$ ,  $\text{CF}^+$ , and  $\text{F}^+$  decrease gradually with the pressure at pressures higher than 5 mTorr, while the density of  $\text{CF}_3^+$  increases with pressure due to the increase in  $\text{CF}_4$  density. In the next section we compare the model results to experimental ones measured by a Langmuir probe.

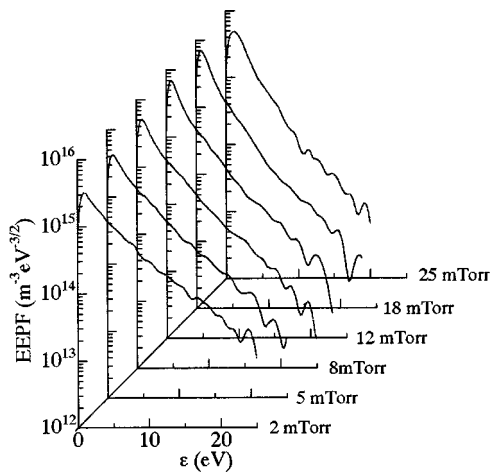
## B. Comparison of model with experiment

In order to use the reaction rates given in Table I, we must verify that the electron energy distributions are nearly Maxwellian over the range of pressures. Experimental results were obtained at a single power of  $P_{\text{abs}} = 70$  W. Some typical results of the EEPF are given in Fig. 2. We see that the distributions are approximately Maxwellian at any pressure, although there is a slight depletion of EEPF at pressures higher than 10 mTorr with respect to a Maxwellian distribution due to the indirect vibrational cross section with a peak value at about 8 eV. On the other hand, a slight enhancement of EEPF at pressures higher than 10 mTorr with respect to a Maxwellian distribution was observed at the energy region lower than 2 to 3 eV. Such an enhancement may be due to the effect of vibrational collision and/or the presence of negative ions. However, such low energy electrons are not important, because these electrons do not play a significant role in the plasma chemistry.

The experimental results estimated from the measured EEPF are compared to the model results from Table IV. Here we estimate  $n_e$  and the effective electron temperature  $T_{\text{eff}}$  as  $n_e = (2/e)^{3/2} (m^{1/2}/A) \int_0^\infty V^{1/2} i_p'' dV$  and  $T_{\text{eff}} = 2/3 \bar{\epsilon}$ , where  $\bar{\epsilon} = \int_0^\infty \epsilon^{3/2} f(\epsilon) d\epsilon / \int_0^\infty \epsilon^{1/2} f(\epsilon) d\epsilon$  is the average electron energy. The comparison of the measured and calculated electron temperatures is shown in Fig. 3(a). The calculated electron temperature may be somewhat larger than the experimental

TABLE IV. Pressure dependence of plasma parameters for charged species with  $P_{\text{abs}} = 70$  W, where all densities are in units of  $10^{16} \text{ m}^{-3}$ .

$p \text{ (mTorr)}$	$n_e$	$T_e \text{ (eV)}$	$V_{\text{sh}} \text{ (V)}$	$\alpha_0$	$\ell_- / \ell_p$	$[\text{CF}_3^+]$	$[\text{CF}_2^+]$	$[\text{CF}^+]$	$[\text{F}^+]$
2	4.35	5.25	26.0	1.19	0.531	2.62	1.31	0.471	0.565
3	4.73	4.77	23.6	1.38	0.536	2.83	1.49	0.548	0.634
5	4.92	4.30	21.3	1.69	0.555	3.14	1.61	0.580	0.646
8	4.73	3.94	19.5	2.12	0.593	3.55	1.54	0.522	0.561
12	4.19	3.64	18.0	2.70	0.651	4.02	1.31	0.399	0.413
18	3.34	3.37	16.7	3.69	0.721	4.51	0.951	0.249	0.247
25	2.62	3.17	15.7	5.00	0.769	4.82	0.661	0.152	0.145
30	2.25	3.08	15.2	6.00	0.788	4.94	0.526	0.113	0.104

FIG. 2. EEPF measured at various pressures with  $P_{\text{abs}} = 70$  W.

temperature due to the deviation of the measured EEPF from the Maxwellian. Good agreement between measured and calculated electron temperatures may lead to good agreement between the measured and calculated sheath voltages shown in Fig. 3(b) because the sheath voltage, which does not strongly depend on the ion mass, is mainly determined by  $T_e$ .

In Fig. 4 we compare the experimental values of  $n_e$  with the model from Table IV. The results indicate reasonable agreement of the magnitude of  $n_e$ , although there still remains a significant difference at pressures lower than 10 mTorr. The near-constant density measured for pressures lower than 20 mTorr is not found in the model, which shows a decrease of  $n_e$  with pressure except at pressures lower than 5 mTorr. The pressure dependence of  $n_e$  in the model is expected because the collisional energy loss per electron-ion pair created is a decrease function of  $T_e$  which means an

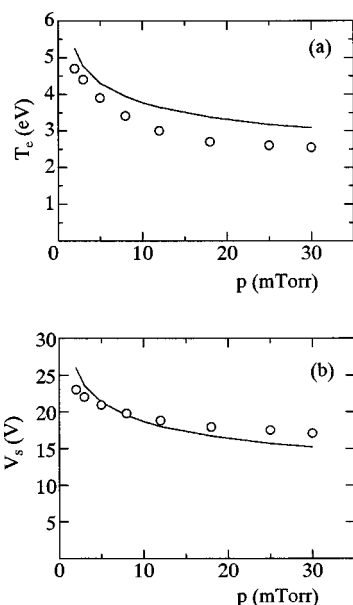
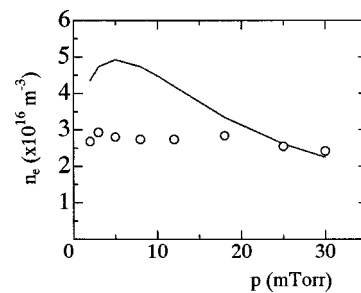


FIG. 3. (a) Comparison of the measured temperature (circles) with the calculated temperature (solid line); (b) comparison of the measured sheath voltage (circles) with the calculated sheath voltage (solid line).

FIG. 4. Comparison of the calculated  $n_e$  (solid line) with the experimental values (circles).

increase function of pressure. However, at low pressure, the effect is so weak that the increase of the loss flux to the wall with the decrease in pressure results in an increasing  $n_e$  with pressure.

## V. CONCLUDING REMARKS

A global model for electronegative plasma, in which the negative ion distribution is assumed to be a parabolic profile in the axial direction with a flat central region and a similar edge profile in the radial direction in the electronegative region, is applied to study the power and pressure dependences of plasma parameters in low-pressure  $\text{CF}_4$  discharges.

The electron density increases approximately linearly with the power. The electron temperature, which is sensitive to the neutral number density, also increases with the power due to the decrease in the neutral number density with increase in power, resulting in the increase in plasma potential. The density of  $\text{CF}_3^+$  is a weak function of the power due to the decrease in  $\text{CF}_4$  density with the increase in power. The density of  $\text{CF}_2^+$  is approximately proportional to the electron density at power higher than 70 W due to the weak power dependence of the densities of  $\text{CF}_3$  and  $\text{CF}_2$ . The variation of  $\text{CF}^+$  and  $\text{F}^+$  densities with the power is faster than that of  $\text{CF}_2^+$ . On the other hand, the decrease in electron temperature with the pressure is significantly responsible for the decrease in the degree of dissociation. The electron density also decreases gradually with the pressure except in the case of pressures lower than 5 mTorr. Such pressure dependence of electron temperature and its density may result in weak pressure dependence of  $\text{CF}_3$  and  $\text{CF}_2$  densities, and the pressure dependence of  $\text{CF}$  and  $\text{F}$  densities which is similar to that of the electron density. Therefore the densities of  $\text{CF}_2^+$ ,  $\text{CF}^+$ , and  $\text{F}^+$  decrease gradually with the pressure at pressures higher than 5 mTorr, while the density of  $\text{CF}_3^+$  increases with the pressure due to the increase in  $\text{CF}_4$  density.

The EEPF is measured with a Langmuir probe in an inductively coupled rf (13.56 MHz)  $\text{CF}_4$  discharge over a pressure range from 2 to 30 mTorr, while keeping the power injected into the plasma at about 70 W. The measured EEPFs are approximately Maxwellian at any pressure, although there is a slight deviation of EEPF at pressures higher than 10 mTorr with respect to a Maxwellian distribution. Good agreement is between measured and calculated electron temperatures, and results in good agreement between the measured and calculated sheath voltages. On the other hand, the

near-constant electron density measured for pressures lower than 20 mTorr is not found from the model, although reasonable agreement of the magnitude of the density is obtained.

## ACKNOWLEDGMENTS

The authors would like to thank Professor A. J. Lichtenberg and Professor M. A. Lieberman of the University of California at Berkeley for valuable discussions and suggestions about the electronegative discharge.

- <sup>1</sup>D. Edelson and D. L. Flamm, J. Appl. Phys. **56**, 1522 (1984).
- <sup>2</sup>I. C. Plumb and K. R. Ryan, Plasma Chem. Plasma Process. **6**, 205 (1986).
- <sup>3</sup>J. P. Booth, G. Hancock, N. D. Perry, and M. J. Toogood, J. Appl. Phys. **66**, 5251 (1989).
- <sup>4</sup>A. Kono, M. Haverlag, G. M. W. Kroesen, and F. J. de Hong, J. Appl. Phys. **70**, 2939 (1991).
- <sup>5</sup>M. Haverlag, A. Kono, D. Passchier, G. M. W. Kroesen, W. J. Goedheer, and F. J. de Hong, J. Appl. Phys. **70**, 3472 (1991).
- <sup>6</sup>J. W. Butterbaugh, D. C. Gray, and H. H. Sawin, J. Vac. Sci. Technol. B **9**, 1461 (1991).
- <sup>7</sup>L. D. B. Kiss and H. H. Sawin, Plasma Chem. Plasma Process. **12**, 523 (1992).
- <sup>8</sup>E. Gogolides, M. Stathakopoulos, and A. Boudouvis, J. Phys. D **27**, 1878 (1994).
- <sup>9</sup>N. V. Mantzaris, A. Boudouvis, and E. Gogolides, J. Appl. Phys. **77**, 6169 (1995).
- <sup>10</sup>E. Gogolides, Jpn. J. Appl. Phys., Part 1 **36**, 2435 (1997).
- <sup>11</sup>S. Segawa, M. Kurihara, N. Nakano, and T. Makabe, Jpn. J. Appl. Phys., Part 1 **38**, 4416 (1999).
- <sup>12</sup>S. Y. So, A. Oda, H. Sugawara, and Y. Sakai, J. Phys. D **34**, 1919 (2001).
- <sup>13</sup>H. Singh, J. W. Coburn, and D. B. Graves, J. Vac. Sci. Technol. A **18**, 2680 (2000).
- <sup>14</sup>H. Singh and D. B. Graves, J. Appl. Phys. **88**, 3889 (2000).
- <sup>15</sup>H. Singh, J. W. Coburn, and D. B. Graves, J. Vac. Sci. Technol. A **19**, 718 (2001).
- <sup>16</sup>H. Singh, J. W. Coburn, and D. B. Graves, J. Vac. Sci. Technol. A **17**, 2447 (1999).
- <sup>17</sup>J. K. Olthoff and Y. Wang, J. Vac. Sci. Technol. A **17**, 1552 (1999).
- <sup>18</sup>Y. Wang, E. C. Benck, M. Misakian, M. Edamura, and J. K. Olthoff, J. Appl. Phys. **87**, 2114 (2000).
- <sup>19</sup>D. B. Hash, D. Bose, M. V. V. S. Rao, B. A. Cruden, M. Meyyappan, and S. P. Sharma, J. Appl. Phys. **90**, 2148 (2001).
- <sup>20</sup>D. Bose, D. Hash, T. R. Govindan, and M. Meyyappan, J. Phys. D **34**, 2742 (2001).
- <sup>21</sup>V. A. Godyak, *Soviet Radio Frequency Discharge Research* (Delphic, Falls Church, 1986).
- <sup>22</sup>C. Lee, D. B. Graves, M. A. Lieberman, and D. W. Hess, J. Electrochem. Soc. **141**, 1546 (1994).
- <sup>23</sup>C. Lee and M. A. Lieberman, J. Vac. Sci. Technol. A **13**, 368 (1995).
- <sup>24</sup>T. Kimura and K. Ohe, Plasma Sources Sci. Technol. **8**, 553 (1999).
- <sup>25</sup>A. J. Lichtenberg, V. Vahedi, M. A. Lieberman, and T. Rognlien, J. Appl. Phys. **75**, 2339 (1994).
- <sup>26</sup>T. Kimura, A. J. Lichtenberg, and M. A. Lieberman, Plasma Sources Sci. Technol. **10**, 430 (2001).
- <sup>27</sup>L. G. Christophorou and J. K. Olthoff, J. Phys. Chem. Ref. Data **28**, 967 (1999).
- <sup>28</sup>L. G. Christophorou, J. K. Olthoff, and M. V. V. S. Rao, J. Phys. Chem. Ref. Data **25**, 1341 (1996).
- <sup>29</sup>V. Tarnovsky and K. Becker, J. Chem. Phys. **98**, 7868 (1993).
- <sup>30</sup>S. Raul and M. J. Kushner, J. Appl. Phys. **82**, 2805 (1997).
- <sup>31</sup>H. Kokura and H. Sugai, Jpn. J. Appl. Phys., Part 1 **39**, 2847 (2000).
- <sup>32</sup>T. R. Hayes, R. C. Wetzel, and R. S. Freund, Phys. Rev. A **35**, 578 (1987).
- <sup>33</sup>J. T. Gudmundsson, J. Phys. D **35**, 328 (2002).
- <sup>34</sup>M. J. Druyvesteyn, Z. Phys. **64**, 781 (1930).